Parametric Analysis of Two-Terminal Impedance-Based Fault Location Methods

Felipe V. Lopes, Kleber M. Silva, and Bernard F. Küsel

***Abstract*—Impedance-based fault location methods have been widely used by utilities to speed up the power supply restoration process after short-circuits in transmission lines. Those techniques based on two-terminal measurements are considered the most reliable ones, since they overcome limitations of single-ended approaches. In this paper, the performances of five digital two-terminal impedance-based fault location methods are evaluated and compared among themselves. In order to do so, a parametric analysis for several fault scenarios in a 500 kV transmission system is carried out in the Alternative Transients Program (ATP), varying quantities which are not commonly analyzed, such as the power system load flow, power factor and system impedance ratio (SIR). The obtained results show that these quantities directly affect the performance of impedance-based fault location methods, highlighting the need to consider them during the evaluation of this type of fault locator.**

***Keywords*: ATP, fault location, fundamental components, impedance-based methods, transmission lines.**

I. Introduction

ELECTRICAL power systems have grown rapidly over the last decades, requiring the increase of the number and length of transmission lines [1]. In this scenario, in cases of short-circuits, a fast and accurate transmission line fault location is essential to reduce the power supply restoration time, which is important with respect to technical and economical issues. Therefore, the study and development of fault locators have been motivated since the 1950s [2], [3].

In the literature on the subject of fault location on power systems, several algorithms have been reported, which are typically divided into four types: Knowledge-based, high-frequency-based, traveling wave-based and impedance-based algorithms. Among them, impedance-based and traveling wave-based approaches are the most used in the field [4]. Traveling wave-based methods have been increasingly used by utilities [5]. These techniques are very reliable and accurate, but require high sampling rates, what makes them more expensive than those based on fundamental frequency components. Therefore, impedance-based fault location methods are still the most used by utilities, since they do not require high sampling frequency rates, greatly improving its simplicity and cost [1].

Among impedance-based fault locators, to locate faults in a given two-terminal line, those devices that use data from both line ends are commonly reported as the most reliable ones. These methods are not affected by fault resistance, as those based on data from one line terminal. There are several types of two-terminal impedance-based fault location methods, whose main differences are on the use of synchronized or unsynchronized data, and on the use of the distributed parameter line model with line shunt capacitances included or the short line model with lumped parameters [1]. Typically, the performance of impedance-based methods is evaluated with respect to the influence of fault characteristics (fault resistance, location and type), data synchronization problems, series compensation or, as found in few works, inaccuracies in transmission line parameters [6]. However, there are other quantities which can directly affect the performance of impedance-based fault locators, but are not normally taken into account, such as the system power flow, the system impedance ratio (SIR) and the system power factor [7].

In this paper, a parametric analysis of five classical two-terminal impedance-based fault location methods is carried out taking into account several operation conditions from the point of view of the system SIR, line power flow and system power factor. To do so, 9118 fault simulations in a 500 kV transmission system were performed in batch mode using the Alternative Transients Program (ATP). For each analyzed operation condition, different fault distances were simulated. The obtained results attest that the performance of impedance-based fault location methods significantly changes when different SIR values, line power flows and system power factors are considered, highlighting the need to analyze these quantities when evaluating impedance-based fault locators.

II. Test Power System Notation and Parameters

Basic concepts and the mathematical formulations of the evaluated fault location algorithms will be presented and briefly analyzed in the next section. These information will be useful to understand the obtained results for each analysis performed. Thus, to facilitate the comprehension of each evaluated fault location technique, the notation of the test power system used as reference here is shown in Fig. 1.

The system consists of a 500 kV transmission line of length ℓ, which connects the sending-end (Bus S) to the receiving-end (Bus R). A communication channel is assumed to be available for data transmission from Bus R to Bus S. $\widehat{V}_F$ is the fundamental voltage phasor at the fault point F, which is d km distant from the Bus S. $\widehat{V}_S$, $\widehat{I}_S$, $\widehat{V}_R$ and $\widehat{I}_R$ represent voltage and current phasors measured at buses S and R, whereas the Thévenin equivalent circuits S1 and S2 represent the power systems connected to each line terminal.

The authors are with Department of Electrical Engineering at University of Brasília (UnB), 70910-900 Brasília, Brazil. (e-mail: felipevlopes@unb.br, klebermelo@unb.br, bernard_kusel@hotmail.com).

Paper submitted to the International Conference on Power Systems Transients (IPST2015) in Cavtat, Croatia, June 15-18, 2015.

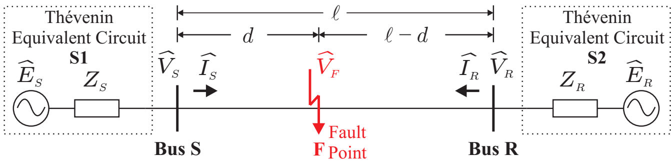

Fig. 1. Test power system single-line diagram.

TABLE I
TRANSMISSION LINE PARAMETERS.

General Data			
Rated Voltage: 500 kV			
Line length ℓ: 200 km			
Line Electrical Parameters			
Sequence	R (Ω/km)	X (Ω/km)	ωC ($\mu\mho/km$)
Zero	0.4930	1.339	2.890
Positive	0.0186	0.267	6.124

The test power system parameters are shown in Tables I and II. From Table II, one can see that the Thévenin equivalent impedance Z_S is multiplied by the variable SIR. It facilitates the simulation of faults considering systems with different SIR values. The default value of the variable SIR is 1. It is varied only to analyze the influence of SIR variations on the implemented two-terminal fault location algorithms. However, during the study of the power flow and power factor influence, SIR = 1, and thus, $Z_S = Z_R$. Also, the Thévenin source values at buses S and R are multiplied by the complex operators $E_S^* \angle \beta_S$ and $E_R^* \angle \beta_R$, respectively, whose default value is $1\angle 0°$. By doing so, one can simulate different line power flows and power factors, by adjusting magnitude and angle values of the operators $E_S^* \angle \beta_S$ and $E_R^* \angle \beta_R$.

III. EVALUATED FAULT LOCATION ALGORITHMS

A. Method GG: Proposed in [8]

In [8], two and three terminal based algorithms are reported. These techniques are able to work using synchronized or unsynchronized data. Here, only the two-terminal approach based on synchronized measurements is analyzed, as it is the most widespread in the literature. This method is based on the lumped parameter line model, in such way that its formulation development takes into account the line series impedance only. Firstly, to obtain the algorithm formulation, $\widehat{V}_F$ is computed considering the fault path at the left side of the system (which contains the source $\widehat{E}_S$), and then, the fault path at the right side of the system (which contains the source $\widehat{E}_R$). Equating both $\widehat{V}_F$ expressions, one can obtain:

$$V_S^{abc} - V_R^{abc} + \ell Z_{abc} I_R^{abc} = d Z_{abc} (I_S^{abc} + I_R^{abc}) \ , \tag{1}$$

where V_F^{abc} is the vector of voltage phasors at the fault point, V_S^{abc}, V_R^{abc}, I_S^{abc} and I_R^{abc} are the vectors of voltage and current phasors at buses S and R, and Z_{abc} is the line series impedance matrix per unit of length, which is computed here from the zero and positive sequence line parameters [9].

TABLE II
THÉVENIN EQUIVALENT CIRCUIT DATA.

Component	Variable	Value
Impedance Z_S	R_1 (Ω)	$3.72 \times$ SIR
	X_1 (Ω)	$53.40 \times$ SIR
	R_0 (Ω)	$98.6 \times$ SIR
	X_0 (Ω)	$267.8 \times$ SIR
Impedance Z_R	R_1 (Ω)	3.72
	X_1 (Ω)	53.40
	R_0 (Ω)	98.6
	X_0 (Ω)	267.8
Sources S1 and S2	$\widehat{E}_S$ (p.u.)	$1.04\angle 8.4° \times E_S^* \angle \beta_S$
	$\widehat{E}_R$ (p.u.)	$1.21\angle -54.5° \times E_R^* \angle \beta_R$

Equation (1) can be rewritten as:

$$Y = M \cdot d \ \text{ or } \begin{bmatrix} Y_a \\ Y_b \\ Y_c \end{bmatrix} = \begin{bmatrix} M_a \\ M_b \\ M_c \end{bmatrix} \cdot d, \tag{2}$$

where

$$M_j = \sum_{i=a,b,c} Z_{ji} (\widehat{I}_S^i + \widehat{I}_R^i), \text{ for } j = a,b,c \ , \tag{3}$$

$$Y_j = \widehat{V}_S^j - \widehat{V}_R^j + \ell \sum_{i=a,b,c} (Z_{ji} \widehat{I}_R^i), \text{ for } j = a,b,c \ . \tag{4}$$

Solving (2) for d and, then, substituting d by the estimated fault distance d_{est}, the fault location can be determined by [8]:

$$d_{est} = (M^+ M)^{-1} M^+ Y \ , \tag{5}$$

where M^+ is the conjugate transpose of M.

For this method, it is important to note that it does not consider the transmission line shunt capacitance effect, what is a source of error that arises mainly in long lines for which the capacitive effect is relevant [1].

B. Method JJ: Proposed in [10]

This algorithm is one of the most accurate techniques available in the literature, since it takes into account the line shunt capacitance effect during the fault location procedure. As a consequence, theoretically, its level of accuracy is the same for short and long lines [7].

The formulation of such technique is also obtained from the computation of $\widehat{V}_F$ considering the fault paths at the left and right sides of the system, but taking into account the distributed parameters of the line. As a consequence, the line propagation constant γ and the characteristic impedance Z_C should be computed [1]. Therefore, by knowing γ, Z_C, the line length ℓ and the voltage and current phasors at line terminals, the estimated fault location d_{est} can be obtained using:

$$d_{est} = \frac{\tanh^{-1}\left[\frac{-\widehat{V}_R \cosh(\gamma\ell) + Z_C \widehat{I}_R \sinh(\gamma\ell) + \widehat{V}_S}{Z_C \widehat{I}_S - \widehat{V}_R \sinh(\gamma\ell) + Z_C \widehat{I}_R \cosh(\gamma\ell)}\right]}{\gamma} . \tag{6}$$

The authors of [10] use as inputs of the algorithm voltage and current modal quantities (aerial-modes), in such a way two estimated fault distances are always obtained. It makes the method dependent on the fault type classification to proper select the excited aerial-mode and, consequently, the correct estimated fault distance. Therefore, for the sake of simplicity, symmetrical quantities are used here, as suggested in [3]. By doing so, only positive sequence quantities are analyzed.

C. Method PR: Proposed in [11]

Method PR is based on synchronized phasor measurements and it does not require the knowledge of line parameters. This characteristic greatly improves the algorithm reliability, since line sequence data normally present inaccuracies [6].

To obtain the formulation depicted in [11], the same analysis of $\widehat{V}_F$ described in the previous sections for the methods GG and JJ is performed, considering only the series impedance of the line (the method is based on the lumped parameter line model). Then, a system of equations which considers the voltage and current positive and negative sequence phasors is created, eliminating line parameters from the formulation. As a result, the estimated fault distance d_{est} can be obtained by:

$$d_{est} = \frac{(\widehat{V}_{S1} - \widehat{V}_{R1})\widehat{I}_{R2} - (\widehat{V}_{S2} - \widehat{V}_{R2})\widehat{I}_{R1}}{(\widehat{V}_{S1} - \widehat{V}_{R1})(\widehat{I}_{S2} + \widehat{I}_{R2}) - (\widehat{V}_{S2} - \widehat{V}_{R2})(\widehat{I}_{S1} + \widehat{I}_{R1})}\ell, \quad (7)$$

where the subscripts '1' and '2' represent positive and negative sequence quantities, respectively.

Method PR does not includes in its formulation the line shunt capacitance effect. Thus, although it is quite simple and reliable, it can present high level of errors when applied to long lines, for which the capacitive current can achieve values comparable of those of currents in the fault path [10]. It should be highlighted that Method PR uses a different approach for symmetrical fault cases, for which, in balanced power systems, negative sequence quantities will not exist [11]. In this paper, only the approach for asymmetrical fault cases is evaluated.

D. Method TZ: Proposed in [12]

This algorithm was developed to locate unbalanced faults. It analyzes two-terminal negative sequence quantities, what overcomes difficulties associated with the pre-fault line load flow and zero sequence mutual coupling effects [12]. Basically, the negative sequence voltage phasor at the fault point is computed considering the fault paths at the left and right sides of the system. Since the method is based on the lumped parameter line model, only the line series impedance is taken into account, resulting in the expression shown next.

$$\widehat{I}_{R2} = \widehat{I}_{S2}\frac{Z_{S2} + mZ_{L2}}{Z_{R2} + (1-m)Z_{L2}}, \quad (8)$$

where the subscripts '1' and '2' represent positive and negative sequence quantities, respectively, Z_{S2} and Z_{R2} are the negative sequence source impedances of the Thévenin equivalent circuits connected to buses S and R, respectively (which are equal to the positive sequence impedances Z_S and Z_R), Z_{L2} is the negative sequence transmission line series impedance (which is equal to the positive sequence line series impedance), and m is the fault distance per unit of length, i.e., $m = \frac{d}{\ell}$.

In order to overcome problems associated to the two-terminal data synchronization process, it is proposed in [12] the use of phasor magnitudes as the algorithm inputs. To do so, the magnitude of both terms in (8) are taken, obtaining:

$$|\widehat{I}_{R2}| = \frac{|(a+jb) + m(c+jd)|}{|(e+jf) - m(g+jh)|}, \quad (9)$$

where:
$\widehat{I}_{S2} \cdot Z_{S2} = a + jb$;
$\widehat{I}_{S2} \cdot Z_{L2} = c + jd$;
$Z_{S2} + Z_{L2} = e + jf$;
$Z_{L2} = g + jh$.

Taking the square of both sides of (9) and rearranging its terms, one can obtain the following quadratic equation:

$$a_2 \cdot m^2 + a_1 \cdot m + a_0 = 0, \quad (10)$$

where:
$a_2 = |I_{R2}|^2 \left(g^2 + h^2\right) - (c^2 + d^2)$;
$a_1 = -2|I_{R2}|^2 \left(e \cdot g + f \cdot h\right) - 2\left(a \cdot c + b \cdot d\right)$;
$a_0 = |I_{R2}|^2 \left(e^2 + f^2\right) - (a^2 + b^2)$.

Solving (10) for m, the fault distance in p.u. is estimated. Multiplying m by the line length ℓ, the estimated fault distance d_{est} is obtained in kilometers. It is important to point out that during the evaluation of this algorithm for cases in which the SIR varies, it will be assumed that the Thévenin equivalent impedances are known with no error.

E. Method HE: Proposed in [13]

The two-terminal fault location reported in [13] is based on the distributed parameter line model, i.e., it takes into account the capacitive effect of the line. The authors of this paper proposes also a technique to dynamically estimate the line parameters during the fault location process. However, here, it will be assumed that line parameters used by each evaluated technique are precise and do not vary.

As in the method JJ, the propagation constant γ and the characteristic impedance Z_C should be computed, before the fault distance estimation process. To improve the method accuracy, the Newton iterative method is used, resulting in very accurate fault point estimations.

The initial value of the estimated fault location d_{est} is represented in [13] by the variable x, which is computed using:

$$x = \frac{\ln\left[\frac{0.5(\widehat{V}_{R1} + \widehat{I}_{R1}Z_C) - 0.5(\widehat{V}_{S1} - \widehat{I}_{S1}Z_C)e^{\gamma\ell}}{0.5(\widehat{V}_{S1} + \widehat{I}_{S1}Z_C)e^{-\gamma\ell} - 0.5(\widehat{V}_{R1} - \widehat{I}_{R1}Z_C)}\right]}{2\gamma}, \quad (11)$$

where the subscript '1' represent positive sequence quantities.

After, the voltage phasor at the fault point is estimated by considering measurements taken from both line ends. Then, the following objective function is obtained:

$$\begin{aligned} F_{dis}(x) &= \widehat{V}_{F1}^S - \widehat{V}_{F1}^R \\ &= \frac{(\widehat{V}_{S1} - \widehat{I}_{S1}Z_C)}{2}e^{\gamma(\ell - x)} + \frac{(\widehat{V}_{S1} + \widehat{I}_{S1}Z_C)}{2}e^{-\gamma(\ell - x)} \\ &\quad - \left(\frac{\widehat{V}_{R1} - \widehat{I}_{R1}Z_C}{2}e^{\gamma x} + \frac{\widehat{V}_{R1} + \widehat{I}_{R1}Z_C}{2}e^{-\gamma x}\right). \end{aligned} \quad (12)$$

To apply the Newton iterative method, one should compute the first-order derivative of $F_{dis}(x)$ with respect to x, which is given by:

$$\begin{aligned}\frac{\partial F_{dis}(x_k)}{\partial x} = & -\gamma\frac{(\widehat{V}_{S1} - \widehat{I}_{S1}Z_C)}{2}e^{\gamma(\ell-x)} \\ & +\gamma\frac{(\widehat{V}_{S1} + \widehat{I}_{S1}Z_C)}{2}e^{-\gamma(\ell-x)} \\ & -\gamma\frac{\widehat{V}_{R1} - \widehat{I}_{R1}Z_C}{2}e^{\gamma x} \\ & +\gamma\frac{\widehat{V}_{R1} + \widehat{I}_{R1}Z_C}{2}e^{-\gamma x}. \end{aligned} \tag{13}$$

Finally, once obtained the initial fault distance estimation $x = x_0$, $F_{dis}(x_0)$ and $\partial F_{dis}(x_0)/\partial x$ are computed and, then, the Newton iterative method can be applied using:

$$x_{k+1} = x_k - \frac{F_{dis}(x_k)}{\frac{\partial F_{dis}(x_k)}{\partial x}}, \tag{14}$$

where x_k is the fault distance estimated in the k^{th} iteration.

If the difference between x_k and x_{k+1} is less than a specified tolerance and the number of iterations results in a period greater than the maximum iteration time, the absolute value of x_{k+1} is taken as d_{est}. Here, the tolerance and maximum iteration number used were of 1E-6 and 5, respectively.

IV. Case Studies

The performance evaluation of the implemented fault location methods was carried out through extensive ATP simulations of AG faults (9118 cases) along the line described in Section II. In each simulation, the voltage and current phasors at buses S and R were obtained from the ATP steady-state solution, ensuring that the phasors used as inputs of the fault location algorithms are from the fault steady-state. During simulations, the line was modeled as a fully transposed line using the distributed parameter line model (PI-Exact line model) with parameters constant in frequency.

The proposed evaluation is divided into three parts: the power flow influence analysis, the SIR influence analysis and the power factor influence analysis. In all cases, solid fault were simulated, varying the fault distance d from 2% to 98% of the line length, with steps of 1%.

A. Power Flow Influence Analysis

To analyze the influence of the line power flow on the implemented algorithms, the operators $E_S^*\angle\beta_S$ and $E_R^*\angle\beta_R$ should be varied, simulating different load angles $\delta = \theta_S - \theta_R$, where θ_S and θ_R are the phase A voltage phasor angles at buses S and R, respectively.

The suitable computation of $E_S^*\angle\beta_S$ and $E_R^*\angle\beta_R$ is crucial to ensure reliable and coherent simulations. To configure them, firstly, the test power system is simulated without the Thévenin impedances, so that voltages at buses S and R are equal to those in the Thévenin sources. Considering voltage magnitudes of 1 p.u. and varying the angles of voltages at buses S and R, the load angle δ can be varied. Once these cases are generated, one can obtain via ATP voltage and current phasors at line terminals, which are then used to compute the Thévenin sources. To do so, Thévenin impedances are reconnected at both line ends, and the Kirchhoff voltage law is applied to obtain the final values of $\widehat{E}_S$ and $\widehat{E}_R$ (Fig. 1).

In this evaluation part, the load angle δ was varied from $-90°$ to $90°$, with steps of $5°$. Although typical values are in the range from $30°$ to $40°$ [14], more adverse cases were simulated to achieve a more comprehensive assessment of the implemented fault location methods. The obtained results are shown in Fig. 2.

From the results, one can see that methods JJ and HE were the most accurate. In fact, these techniques takes into account the line capacitive effect, making them to be accurate even when applied to very long lines [7]. Methods GG, PR and TZ also presented good performance in most simulated cases. For methods GG and TZ, the fault location errors did not exceed the order of few kilometers. However, the method PR resulted in relevant errors for load angles close to zero. It is due to some terms of this technique formulation, which are proportional to the difference between positive and negative sequence voltage phasors at the line ends (see (7)). Thus, for $\delta = 0°$, these terms present very small values, leading the fault locator to misoperate. Even so, for typical values of δ, the method PR showed to be accurate, resulting in errors which did not exceed the order of 3 km.

An important aspect to be analyzed here is the influence of the line power flow associated with variations in the fault distance. From Fig. 2, it is noticed that methods GG, TZ and HE are very robust to the line power flow, but are influenced by the fault distance. On the other hand, methods JJ and PR are more sensitive to power flow variations. As mentioned before, the obtained results using the method PR can present unacceptable errors for $\delta \approx 0°$, whereas, for this same condition, the method JJ presents a very good performance.

B. SIR Influence Analysis

The SIR is a quantity given by the relation between the Thévenin impedance and the line series impedance. For the analyzed test power system, it is computed by $\frac{Z_S}{\ell Z_{L1}}$, where Z_{L1} is the positive sequence line series impedance per unit of length. Typically, SIR variations can have influence on several protection algorithms, such as the impedance-based and traveling wave-based fault location techniques [1]. However, only few papers consider such influence, what motivated us to present this analysis here.

To evaluate the SIR influence on the implemented methods, the Thévenin impedance connected to Bus S was varied. SIR values equal to 0.1, 0.2, 0.3, ..., 0.8, 0.9, 1, 2, 3, ..., 9 and 10 were simulated such as described in Table II. For this case, the default value of the operators $E_S^*\angle\beta_S$ and $E_R^*\angle\beta_R$ was used, resulting in Thévenin sources equal to $\widehat{E}_S = 1.04\angle 8.4°$ p.u. and $\widehat{E}_R = 1.21\angle -54.5°$ p.u.. It is important to point out that the method TZ depends on the Thévenin impedance, as described in Section III-D. Thus, to provide a fair assessment of the implemented methods, in this analysis, it was assumed that the Thévenin impedance Z_S is known by the method TZ with no error. In other words, the algorithm knows the correct SIR value simulated in each case.

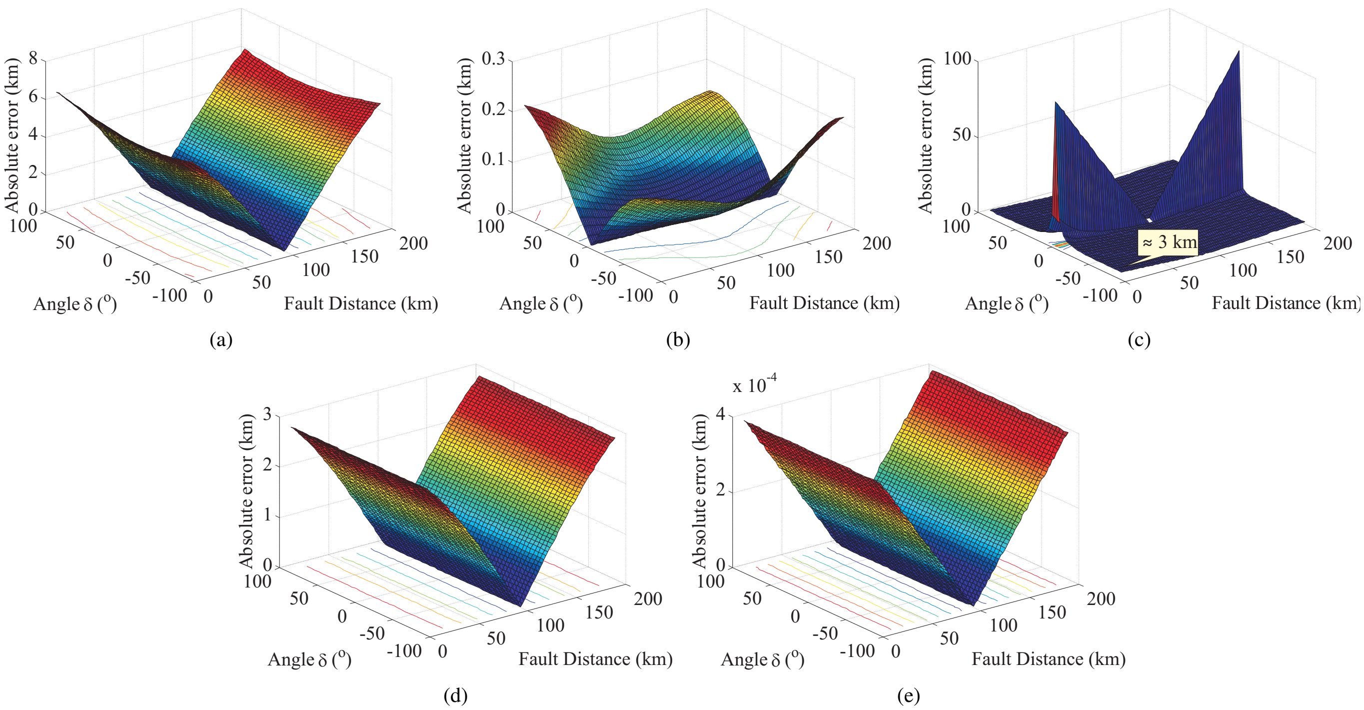

Fig. 2. Power flow influence analysis: (a) Method GG; (b) Method JJ; (c) Method PR; (d) Method TZ; (e) Method HE.

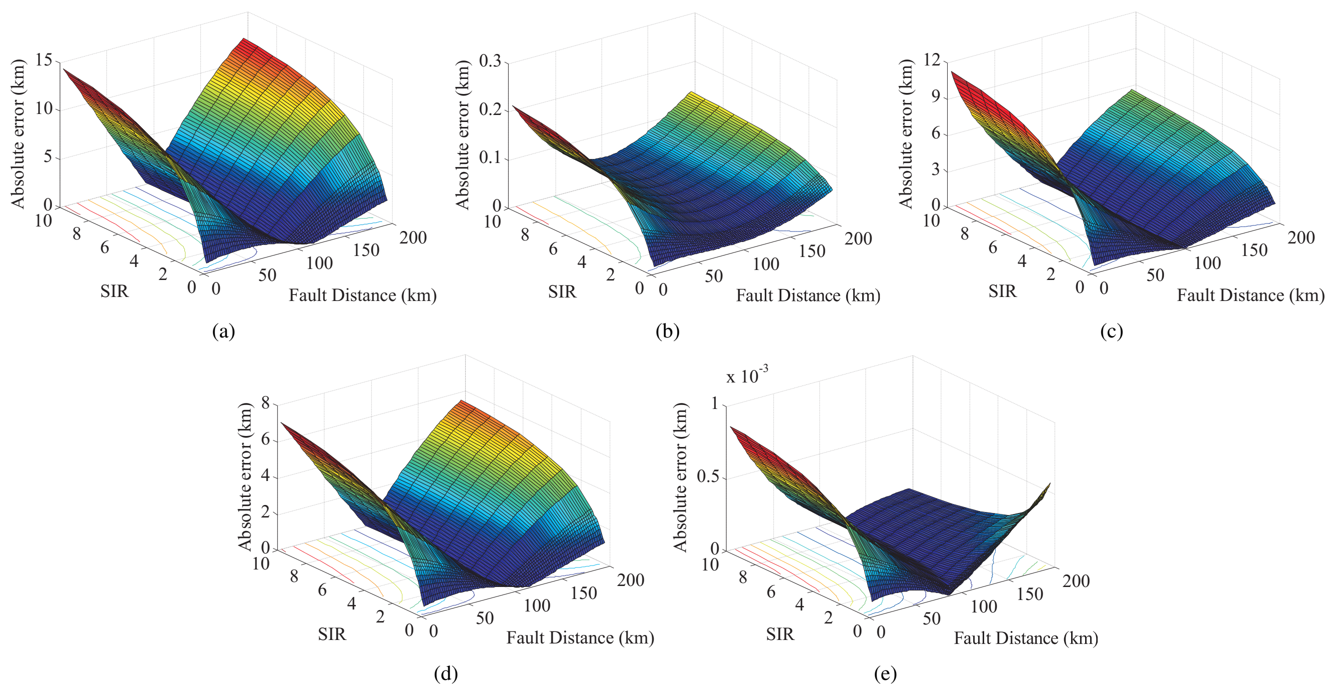

Fig. 3. SIR influence analysis: (a) Method GG; (b) Method JJ; (c) Method PR; (d) Method TZ; (e) Method HE.

The obtained results are shown in Fig. 3. One can notice that the performances of the evaluated techniques change with the SIR variation. From the results, it can be seen that the worse cases were associated to close-in faults when the SIR has high values. For these cases, the fault distances estimated using the methods GG, PR and TZ presented maximum errors of the order of 15 km, 12 km and 8 km, respectively. For faults close to the middle of the line, good performances were observed, reducing the fault location errors for values smaller than 1 km. It should be highlighted that the method TZ achieved this level of accuracy only because the SIR value was adjusted in the algorithm at each simulation. An additional analysis was carried out to compute the maximum error of such technique if the Thévenin impedance default value is considered. Errors in the order of 300 km were obtained, attesting that relevant SIR variations can jeopardize its accuracy and reliability.

Methods JJ and HE also showed to be influenced by SIR variations. Even so, again, these techniques were the most accurate ones, providing fault distance estimations with maximum errors of the order of 0.2 km and 1 m, respectively. In a broad perspective, one can conclude that the evaluated techniques presented behaviors similar among themselves when the SIR was varied. In fact, for small SIRs, the influence of the fault distance is less relevant if compared with those cases for which the SIR is high. For instance, in fault cases in which SIR ≈ 0, the maximum fault location error obtained through the method GG was of about 2.5 km, whereas in cases in which SIR ≈ 10, the maximum error was of about 15 km.

C. Power Factor Influence Analysis

To perform the power factor influence analysis, the operators $E_S^* \angle \beta_S$ and $E_R^* \angle \beta_R$ should be varied. To configure these operators, a set of procedures are needed before simulating the power system. Basically, the voltage at Bus S is assumed to be $1\angle 0°$ p.u., whereas the current in this same bus is defined in accordance to the power factor values which will be analyzed. Then, since voltage and current at Bus S are known, Thévenin sources at both line ends can be computed, i.e., the operators $E_S^* \angle \beta_S$ and $E_R^* \angle \beta_R$ are obtained. Finally, the test power system is simulated, associating each obtained Thévenin source to each evaluated power factor.

In this evaluation part, the power factor at Bus S was varied from 0.1 to 1.0, with steps of 0.05. Lagging and leading power factors were simulated. In transmission systems, the power factor can vary a lot, what has motivated this analysis. The obtained results are shown in Figs. 4 and 5.

From the obtained results, one can see that the level of errors in both lagging and leading power factor cases were similar. All methods showed to be robust to power factor variations. Only the methods JJ and PR presented a more evident sensitivity to it. Even so, this behavior did not compromise the method JJ performance, which resulted in errors smaller than 60 m. The method PR also demonstrated to be slightly influenced by power factor variations. This behavior can be observed mainly in cases of close-in faults. Even so, the level of accuracy of this algorithm was better than those observed in the previous sections, highlighting its robustness in power system in which the power factor often varies. In this context, it should be pointed out that the methods GG, TZ and HE showed to be even more robust than the methods JJ and PR. The performances of these techniques were almost constant for each fault distance, attesting that the power factor does not have significant influence on their level of accuracy.

D. Additional Remarks

From the obtained results in the previous sections, it was proved that two-terminal impedance-based fault locators are influenced by the line power flow, SIR variations and system power factors. Among these quantities, the line power flow and SIR variations were the ones that have produced the biggest fault location errors.

For the sake of space limitation, the power flow, SIR and power factor were analyzed in relation to the fault distance only. From this study, it was observed that the fault distance determines the level of influence of these quantities on the analyzed fault location algorithms. Thus, in future works, it is intended to analyze again the methods GG, JJ, PR, TZ and HE, but evaluating the influence of the power flow, SIR and power factor with each other and in relation to the fault features.

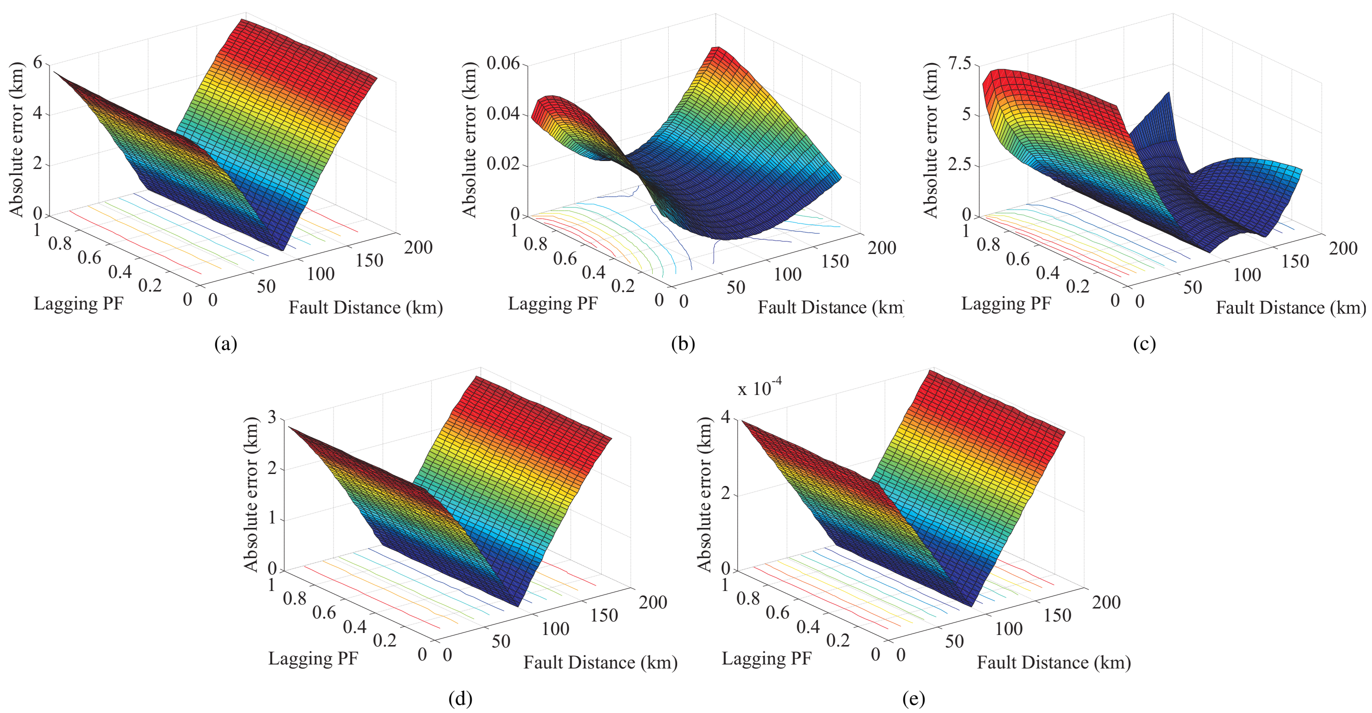

Fig. 4. Lagging power factor influence analysis: (a) Method GG; (b) Method JJ; (c) Method PR; (d) Method TZ; (e) Method HE.

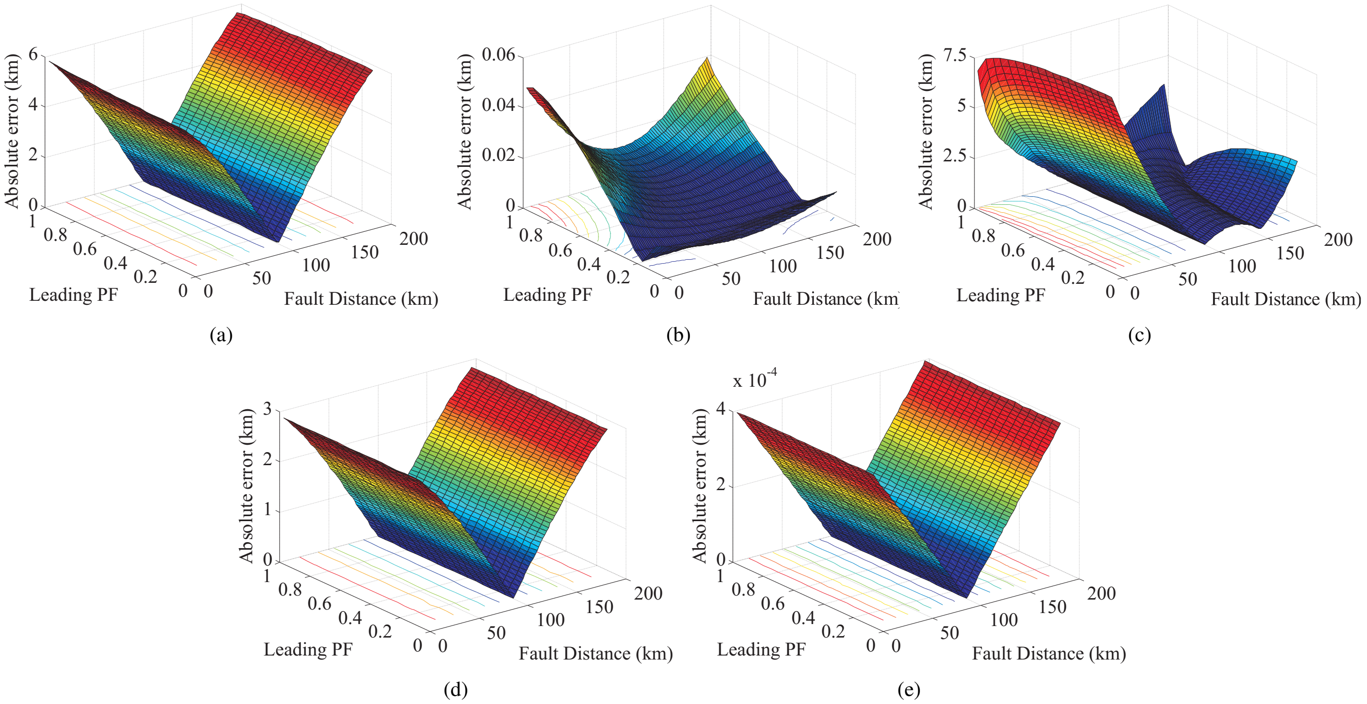

Fig. 5. Leading influence analysis: (a) Method GG; (b) Method JJ; (c) Method PR; (d) Method TZ; (e) Method HE.

V. Conclusions

In this paper, five digital two-terminal impedance-based fault location methods were thoroughly evaluated, considering the influence of quantities which are not normally taken into account in papers, such as the line power flow, SIR and system power factor. The influence of these quantities were analyzed for different fault distances. A total amount of 9118 solid AG fault cases in a 500 kV transmission system were simulated using the ATP. For each case, the fault location errors were computed and presented as surfaces in which the X axis is the fault distance, the Y axis is the analyzed quantity (power flow, SIR or power factor) and the Z axis is the absolute error.

Among the evaluated methods, three are based on the lumped parameter line model and two are based on the distributed parameter line model. The algorithms showed to be significantly influenced by the line power flow and SIR variations. Only two of the evaluated techniques demonstrated a certain sensitivity to power factor variations, which was not enough to compromise their performances. From the simulations, it was concluded that the fault distance determines in most cases the level of influence of the power flow, SIR and power factor on the fault location algorithms, what proves that these quantities should be taken into account during the evaluation of two-terminal impedance-based fault locators.

VI. References

[1] M. M. Saha, J. Izykowski, and E. Rosolowski, *Fault Location on Power Networks*, ser. Power Systems. London: Ed. Springer, 2010.

[2] T. W. Stringfield, D. J. Marihart, and R. F. Stevens, "Fault location methods for overhead lines," *Transactions of the American Institute of Electrical Engineers Power Apparatus and Systems, Part III.*, vol. 76, no. 3, pp. 518 –529, april 1957.

[3] A. Dalcastagne and S. Zimath, "A study about the sources of error of impedance-based fault location methods," in *2008 IEEE/PES Transmission and Distribution Conference and Exposition: Latin America*, aug. 2008, pp. 1 –6.

[4] A. G. Phadke and J. S. Thorp, *Computer Relaying for Power Systems*, 2nd ed. New York, USA: John Wiley & Sons Inc, 2009.

[5] S. L. Zimath, M. A. F. Ramos, and J. E. S. Filho, "Comparison of impedance and travelling wave fault location using real faults," in *2010 IEEE PES Transmission and Distribution Conference and Exposition*, April 2010, pp. 1 –5.

[6] F. V. Lopes, D. Fernandes Jr., W. L. A. Neves, and Y. Melo, "Real-time evaluation of PMU-based fault locators," *International Conference on Power Systems Transients (IPST2013)*, July 2013.

[7] F. V. Lopes, B. F. Küsel, K. M. Silva, D. Fernandes Jr, and W. Neves, "Fault location on transmission lines little longer than half-wavelength," *Electric Power Systems Research*, vol. 114, pp. 101–109, 2014.

[8] A. Girgis, D. Hart, and W. Peterson, "A new fault location technique for two- and three-terminal lines," *IEEE Transactions on Power Delivery*, vol. 7, no. 1, pp. 98–107, Jan. 1992.

[9] H. W. Dommel, *Electromagnetic Transients Program Reference Manual: EMTP Theory Book*, Portland, BPA, 1996.

[10] A. Johns and S. Jamali, "Accurate fault location technique for power transmission lines," *IEE Proceedings C Generation, Transmission and Distribution*, vol. 137, no. 6, pp. 395–402, Nov. 1990.

[11] G. Preston, Z. Radojevic, C. Kim, and V. Terzija, "New settings-free fault location algorithm based on synchronised sampling," *IET Generation, Transmission and Distribution*, vol. 5, no. 3, pp. 376–383, 2011.

[12] D. Tziouvaras, J. Roberts, and G. Benmouyal, "New multi-ended fault location design for two- or three-terminal lines," in *Seventh International Conference on (IEE) Developments in Power System Protection, 2001*, 2001, pp. 395–398.

[13] Z. He, R. Mai, W. He, and Q. Qian, "Phasor-measurement-unit-based transmission line fault location estimator under dynamic conditions," *IET Generation, Transmission and Distribution*, vol. 5, no. 11, pp. 1183–1191, 2011.

[14] H. Saadat, *Power System Analysis*. Michigan: McGraw-Hill, PSA Publishing, 1999.